Nuclear Science and Techniques (2026) 37:33
https://doi.org/10.1007/s41365-025-01835-9

Strain-related phenomena in GaN epilayers under MeV inert gas ion irradiation

Li-Qing Zhang[1,2] · Yang Gao[1] · Shuang Liu[1] · Qin-Wei Wang[1] · Ya-Xun Zhang[1] · Rui Li[1] · Chong-Hong Zhang[2] · Lei Zhou[1] · Qiang Zhou[1] · Chen-Chun Hao[1] · Rong Qiu[1]

Received: 20 May 2024 / Revised: 12 August 2024 / Accepted: 16 August 2024 / Published online: 5 January 2026

Abstract
Single-crystal GaN epilayers were irradiated with heavy inert gas ions (2.3-MeV Ne^{8+}, 5.3-MeV Kr^{19+}) to fluences ranging from 1.0×1.0^{11} to 1.0×1.0^{15} ions/cm^2. The strain-related damage accumulation versus ion fluences was studied using high-resolution X-ray diffraction (HRXRD) and ultraviolet–visible (UV–Vis) spectroscopy. The results showed that the damage accumulation was mainly dominated by nuclear energy loss. When the ion fluence was less than ~ 0.055 displacement per atom (dpa), the lattice expansions and lattice strains markedly increased linearly with increasing ion fluences, accompanied by a slow enhancement in the dislocation densities, distortion parameters, and Urbach energy for both ion irradiations. Above this fluence (~ 0.055 dpa), the lattice strains presented a slight increase, whereas a remarkable increase was observed in the dislocation densities, distortion parameters, and Urbach energy with the ion fluences after both ion irradiations. ~ 0.055 dpa is the threshold ion fluence for defect evolution and lattice damage related to strain. The mechanisms underlying the damage accumulation are discussed in detail.

Keywords GaN · Gas ion irradiation · HRXRD · UV–Vis spectra · Strains · Urbach energy

1 Introduction

Gallium nitride (GaN) with a hexagonal structure exhibits strong covalent bonds between gallium (Ga) and nitrogen (N) atoms. The binding energy of the Ga–N bond in GaN is approximately 8.92 eV per atom [1]. This property contributes to its high melting point, high acid and alkali resistance, high thermal conductivity, excellent anti-radiation properties, and excellent mechanical stability. Compared with other semiconductor materials (Si, Ge, InP, GaAs, and ZnO) [2–5], GaN possesses excellent electrical and optical properties, such as a wide band gap, high breakdown field (voltage), high electron mobility, and high saturated electron drift velocity. Consequently, GaN has received increasing attention owing to its superior characteristics. Currently, GaN is regarded as a typical third-generation semiconductor material, similar to Si and GaAs. It is widely used in optoelectronics, power electronics, and other fields. It has promising potential for use in ultraviolet detectors, short-wavelength light-emitting diodes (LEDs), laser diodes (LDs), high-electron-mobility transistors (HEMTs), heterojunction bipolar transistors (HBTs), and high-frequency, high-power, high-temperature electronic devices [6–9]. Notably, the significant radiation endurance of GaN makes it particularly suitable for harsh environments with high irradiation fluences because its amorphization threshold is much higher. Therefore, GaN-based devices are typically utilized as detectors or lighting in harsh environments, such as aviation, aerospace, nuclear industries, and nuclear power plants [10]. During service, these devices inevitably suffer from radiation damage caused by cosmic rays and various

This work was supported by the Program for National Natural Science Foundation of China (No. 11675231), the Sichuan Science and Technology Program (Nos. 2022YFG0263 and 2024NSFSC1097), and the Scientific Research Starting Foundation for talents (Nos. 21zx7109 and 22zx7175, 24ycx1005).

✉ Li-Qing Zhang
liqingzhang07@163.com

[1] Joint Laboratory for Extreme Conditions Matter Properties, Southwest University of Science and Technology, Mianyang 621010, China

[2] Institute of Modern Physics, Chinese Academy of Sciences, Lanzhou 730000, China

energetic particles (protons, electrons, neutrons, swift heavy ions, and highly charged ions). In the irradiation-induced damage of GaN materials by keV energy ions, the ion energy is believed to be transferred mainly through ion–atom nuclear collisions, which is quantified by the nuclear energy loss. Meanwhile, in the irradiation-induced damage of GaN materials by MeV energy ions, the ions deposit most of their energy via electronic excitation and ionization of atoms along their trajectories, which is quantified by the electron energy loss [11–18].

Regardless of the cascade collision or excitation/ionization processes, once the deposited energy of the ions exceeds the displacement threshold energy of the atoms in GaN materials, point defects such as vacancies and interstitials are generated. Thus, the long-range order of the GaN lattices is destroyed, which is accompanied by lattice strain. Corresponding changes in the optical characteristics of GaN occur because of the interaction between the defects/disordered lattices and carriers. Its optical properties are very sensitive to the nature and level of point and/or extended defects. With the accumulation of point defects, the increasing disorder of the lattice atoms intensifies the distortion of lattice planes in conjunction with the occurrence of defect evolution related to the strain. The irradiation-induced damage accumulation, lattice strain, defect evolution, and change in the optical characteristics of GaN materials and devices have been extensively investigated [18–33]. For keV energy ions, nuclear energy loss plays an important role in irradiation-induced damage in GaN materials. For MeV energy ions, the energy deposition processes in GaN materials depend not only on the kinetic energy of the incident ions but also on their volumes [34]. Sometimes, the irradiation damage of MeV energy ions in GaN is mainly ascribed to nuclear energy loss, not electron energy loss. Therefore, the effects of different energy losses in GaN in the case of irradiation with MeV energy ions is an important issue that needs to be clarified. Moreover, inert gas ions do not bond with Ga and N atoms but produce defects.

In the present work, to study the predominant effect of electron energy loss and nuclear energy loss of MeV energy ions in the microstructures, lattice strains, and optical properties of GaN materials, we performed irradiation experiments of GaN films with 2.3 MeV $^{20}Ne^{8+}$ and 5.3 MeV $^{84}Kr^{19+}$ ions at different fluences. The specimens were analyzed using high-resolution X-ray diffraction and ultraviolet visible spectroscopy.

2 Experiment

The specimens used in this study were n-type wurtzite GaN layers grown on c-plane sapphire via metal–organic chemical vapor deposition (MOCVD) with a doping concentration of 1.0×10^{17} Si/cm^3. Their thickness was approximately 3.0 μm. The irradiation experiment was performed at a terminal of the 320 kV high-voltage atomic physics experimental platform with an ECR ion source at the Institute of Modern Physics (IMP), China. The specimens were irradiated with 2.3-MeV $^{20}Ne^{8+}$ ions to successively increasing fluences of 1.0×10^{11}, 1.0×10^{12}, 1.0×10^{13}, 1.0×10^{14}, and 1.0×10^{15} Ne^{8+} ions/cm^2, and were irradiated with 5.3-MeV $^{84}Kr^{19+}$ ions to fluences of 1.0×10^{11}, 1.0×10^{12}, and 1.0×10^{13} Kr ions/cm^2, in a vacuum of approximately 5×10^{-5} Pa at ambient temperature. To avoid the obvious heating effect caused by the ion beams, the ion flux was controlled to below 1×10^{11} ions/cm^2/s. The projected ion ranges and electronic and nuclear stopping powers in the GaN material under these conditions of irradiation with the two types of ions were estimated using the SRIM 2013 code [34]. The calculated ion ranges

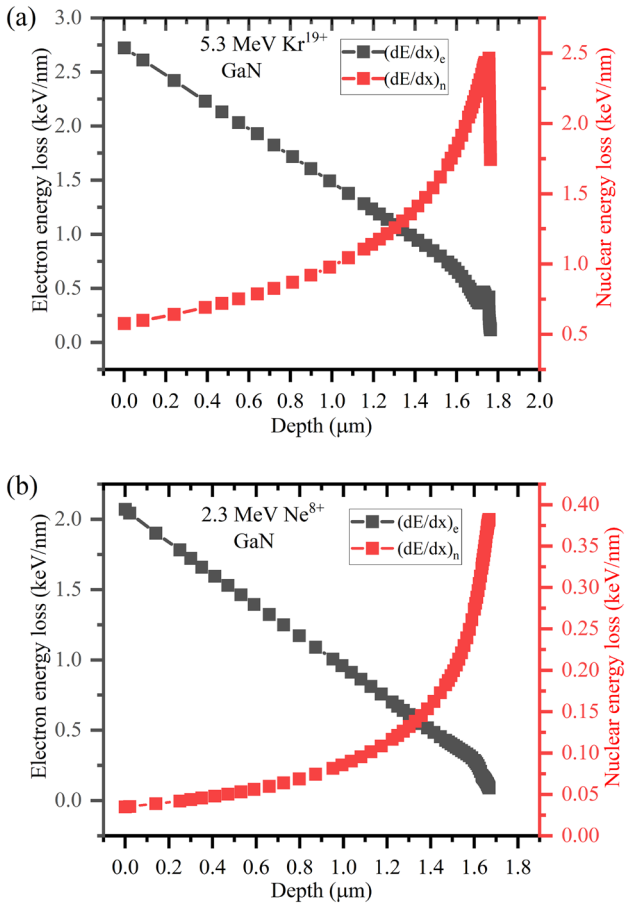

Fig. 1 (Color online) Electron energy loss, nuclear energy loss, and ion range of (**a**) 5.3-MeV Kr^{19+} ions and (**b**) 2.3-MeV Ne^{8+} ions in GaN obtained using the SRIM 2013 code

and energy losses are shown in Fig. 1a and b. In Fig. 1, the incident ion range is approximately 1.78 and 1.68 μm for 5.3-MeV Kr^{19+} and 2.3-MeV Ne^{8+} ions, respectively. They rest in the GaN epilayers for the two types of ions. For the 5.3-MeV Kr^{19+} ions in GaN, the electron and nuclear energy losses are of the same order of magnitudes. Their maximum values are 2.75 and 2.49 keV/nm, respectively. For the 2.3-MeV Ne^{8+} ions in GaN, the electron energy loss was approximately five times larger than the nuclear energy loss. Their maximum value is 2.15 and 0.38 keV/nm, respectively. Meanwhile, the damage distribution and atom concentration in all the GaN specimens were calculated from SRIM "quick calculations". The energies for displacement were set to 20.8 eV and 10.5 eV for the Ga and N atoms, respectively [35]. Under 5.3-MeV Kr^{19+} irradiation at a fluence of 1.0×10^{11} Kr^{19+} ions/cm^2, the calculated peak of atomic displacement levels in displacement per atom (dpa) and the atom concentration were 2.5×10^{-4} dpa and 1.6×10^{-2} appm, respectively. As the ion fluence increased to 1.0×10^{12} Kr^{19+} ions/cm^2, the peak values of the displacement damage and atom concentration increased to 2.5×10^{-3} dpa and 1.6×10^{-1} appm, respectively. At the highest fluence (1.0×10^{13} Kr^{19+} ions/cm^2) irradiation, the corresponding calculated peak values of displacement damage and atom concentration were 2.5×10^{-2} dpa and 1.6 appm, respectively. For 2.3-MeV Ne^{8+} ion irradiation at fluences of 1.0×10^{11}, 1.0×10^{12}, 1.0×10^{13}, 1.0×10^{14}, and 1.0×10^{15} Ne^{8+} ions/cm^2, the calculated peak values of the displacement damage were approximately 5.3×10^{-5}, 5.3×10^{-4}, 5.3×10^{-3}, 5.3×10^{-2}, and 5.3×10^{-1} dpa, respectively, and the atom concentrations were approximately 2.57×10^{-2}, 2.57×10^{-1}, 2.57, 2.57×10^{1}, and 2.57×10^{2} appm, respectively.

After irradiation, all GaN specimens, including the unirradiated and irradiated samples, were measured using high-resolution X-ray diffraction (HRXRD) and ultraviolet–visible transmittance spectroscopy (UV–Vis). The HRXRD measurements were performed using a D8 Discover X-ray diffractometer. It was equipped with a four-crystal monochromator in a Ge(220) configuration and one or two 200 μm slits before the detector. Monochromatic Cu Kα1 X-rays ($\lambda = 0.15406$ nm) were used as the incident light. $\omega/2\theta$ scanning was performed on the (0002) lattice planes of all GaN specimens. $\omega/2\theta$ scanning was performed with a step length of 0.001° using a Ge(220) three-axis analyzing crystal set.

The UV–visible transmittance spectra were measured using a Lambda 900 UV/Vis/NIR spectrometer by PerkinElmer Inc. Wolfram and deuterium lamps were used as incident lights. The spectral resolution is 1 nm. Transmittance spectra were recorded from 200 to 2500 nm wavelength regions.

3 Results and discussion

3.1 HRXRD analysis

Figure 2 shows $\omega/2\theta$ scanning curves and strain distribution analysis of the GaN(0002) lattice plane irradiated with 5.3-MeV Kr^{19+} and 2.3-MeV Ne^{8+} at different fluences. The measured lattice constant c of the original specimen was 0.5188 nm, which is slightly larger than the standard value of 0.5185 nm. This difference is attributed to the biaxial stress between the epitaxial GaN films and sapphire substrates [36, 37].

The $\omega/2\theta$ scanning results for GaN irradiated with the two types of ions exhibited the same trend. The diffraction peak shifted regularly to smaller angles as the ion fluence

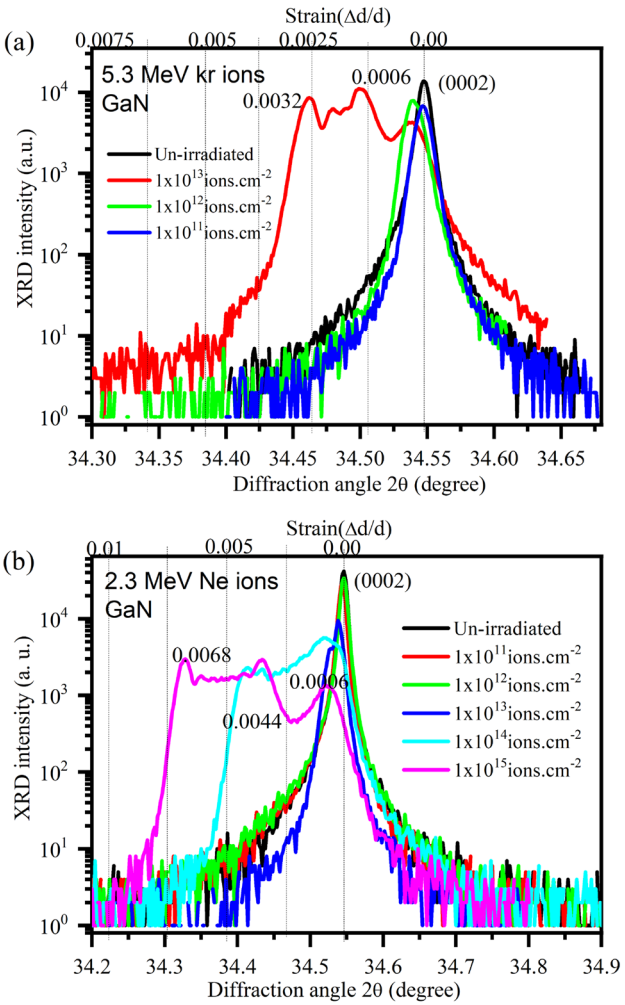

Fig. 2 (Color online) ω ~2θ scanning profiles and strain distribution analysis of GaN (0002) lattice plane irradiated with (**a**) 5.3-MeV Kr^{19+} ions and (**b**) 2.3-MeV Ne^{8+} ions at different fluences

increased, and increasing broadening of the diffraction peak was observed with increasing ion fluence. Moreover, a split in the main peak occurred and several satellite peaks beside the main peak appeared at relatively higher fluences (Fig. 2a and b). The appearance of these small peaks at lower angles was due to the expansion of the original lattices and the generation of new crystal planes, and the extinction of some small peaks was due to the distortion of new crystal planes or the occurrence of partial amorphization for higher fluence irradiation. Similar phenomena were observed in Ar ion-irradiated GaN specimens [37]. These were also ascribed to defect creations in the crystal structure, which led to lattice expansion and variation in the interplanar distance. The lattice expansion can be calculated using Bragg's law, $2d\sin\theta = j\lambda$ ($\lambda = 0.15406$ nm and θ is the diffraction angle of the HRXRD curves). Furthermore, these were also attributed to the buildup of lattice compression and lattice strain in GaN films by the energy deposition of incident ions [37–39]. In addition, the broadening of the diffraction peaks indicated that the introduced stress was not uniformly distributed and that a depth distribution with a continuously varying damage level was formed.

To determine the weight of the two types of energy deposition via electronic excitation/ionization or nuclear collision processes in the production of damage in GaN, the $\omega/2\theta$ scanning curves between the two different types of ions were compared. In the SRIM 2013 estimates (Fig. 1), we can observe that along the entire range of incident ions, at the same ion fluence, the electronic energy deposition of a Kr ion is approximately 1.5 times that of a Ne ion, whereas the nuclear energy deposition of a Kr ion is approximately 5 times that of a Ne ion. The diffraction peak corresponding to the smallest diffraction angle shown in Fig. 2 is from the region of the damage peak induced by the displacement damage owing to nuclear energy deposition.

In addition to the lattice expansion and interplanar spacing changes, lattice strain can be deduced from the HRXRD curves. Based on Hooke's law, the value of $\Delta d/d$ characterizes lattice strain. This is obtained from the differential form of Bragg's equation [40, 41].

$$\left(\frac{\Delta d}{d}\right) \approx \Delta\theta \times \cot\theta_{\text{Bragg}}, \tag{1}$$

where $\Delta\theta$ is the difference between the diffraction angle and Bragg angle. The smallest diffraction angle was selected for calculating $\Delta\theta$ and Δd in the HRXRD curves. After 5.3-MeV Kr^{19+} ion irradiation, significant lattice strains with values of 0.00005, 0.0006, and 0.0032 were generated for 1.0×10^{11}, 1.0×10^{12}, and 1.0×10^{13} Kr ions/cm^2 irradiation, respectively (Fig. 2a). Meanwhile, for 2.3-MeV Ne^{8+} ion irradiation at fluences of 1.0×10^{11}, 1.0×10^{12}, 1.0×10^{13}, 1.0×10^{14}, and 1.0×10^{15} Ne ions/cm^2, the corresponding strain values were 0, 0.00008, 0.0006, 0.0044, and 0.0068, respectively (Fig. 2b).

To investigate the dependence of lattice strains on ion fluences in the GaN specimens, we also determined the relationship between the lattice strain ($\Delta d/d$) and dpa levels in Fig. 3 after the GaN specimens were irradiated with Kr^{19+} and Ne^{8+} ions with different fluences. Moreover, data for GaN irradiated with 100 keV Si ions at different fluences from the work of Qadri et al. [42] are also included in Fig. 3. The dpa level is a measure of atomic displacement due to nuclear collision processes. For the diffraction patterns with more than one peak in the HRXRD curves, the peak with the smallest diffraction angle was selected to calculate Δd. The curve for 2.3 MeV Ne^{8+} ion-irradiated GaN was coincident with that of 5.3 MeV Kr^{19+} ion-irradiated GaN and was in good agreement with that of 100 keV Si^+ ion-irradiated GaN (Fig. 3). In other words, the strains in GaN induced by the three ions (Kr^{19+}, Ne^{8+}, and Si^+) displayed the same trend (Fig. 3). The lattice strain ($\Delta d/d$) in the GaN specimens increases with the dpa levels generally (Fig. 3). This further verifies that nuclear energy loss is the main reason for damage production in the peak dpa region in GaN in the present cases of ion irradiation. The electronic energy loss (below 3 keV/nm/ion can be ignored in this experiment.

Meanwhile, it is noticeable that the strain value ($\Delta d/d$) increases in an approximately linear proportion with the value of dpa when the dpa value is less than ~0.055, whereas

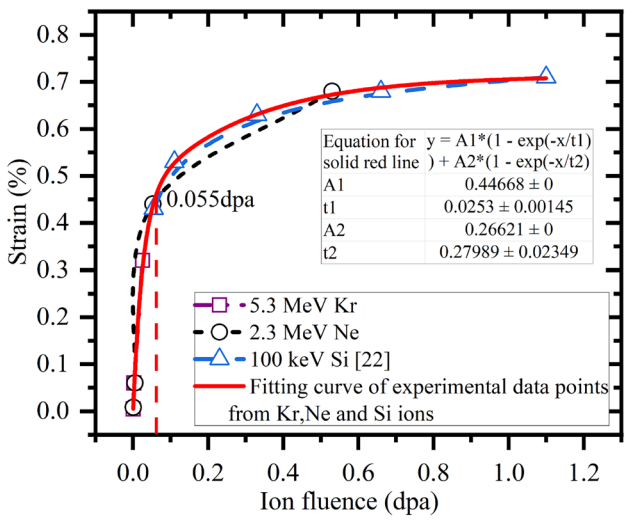

Fig. 3 (Color online) Strain as a function of displacement per atom (dpa) level for GaN films irradiated with Kr^{19+}, Ne^{8+}, and Si^+ ions at different fluences, where the solid red line is a fitting curve of experimental data points from three ions (Kr^{19+}, Ne^{8+}, and Si^+). The purple, black, and blue dashed with open symbols lines denote variations of strain versus fluence (dpa), corresponding to the Kr^{19+}, Ne^{8+}, and Si^+ irradiated specimens, respectively. The vertical dashed red line points to the value of ~ 0.055 dpa

it increases more slowly as the value of dpa increases above ~0.055, as shown in Fig. 3. This turning point at approximately ~ 0.055 dpa is regarded as a transfer between the two stages of defect accumulation in GaN. When the damage accumulation via nuclear energy loss is lower than a certain level, defects in GaN are almost point type, and there is no overlap of the individual damage zones produced by each incident ion. In the case of a low damage level, the dpa value, concentration of point defects, and stress and strain built up in GaN are linearly correlated with each other. Here, ~ 0.055 dpa is assumed to be the threshold value above which point defects become saturated and begin to combine with each other to form more complex types. The evolution of defects was responsible for the behavior of the strain ($\Delta d/d$) at dpa levels above 0.055. Moreover, the fitting curve of strain versus fluence (dpa) was obtained by fitting the strain data of the three ions (Kr^{19+}, Ne^{8+}, and Si^{+}) in GaN materials at different fluences in Fig. 3. The fitting curve equation was also used to characterize the dependence of strains in GaN films on the dpa level. The fitting equation is as follows:

$$\varepsilon = 0.4467(1 - e^{-39.53\phi}) + 0.2662(1 - e^{-3.573\phi}), \quad (2)$$

where ε is the strain and ϕ is the ion fluence (dpa). As can be observed from Eq. (2), the strain in GaN films is primarily composed of two parts after irradiation at different fluences. Based on the displacement damage and ion concentration distributions after irradiation, we conclude that the strains, as expressed in Eq. (2), are mainly defect-induced and incident-ion-induced strains, respectively. Defect-induced strains arise from displacement damage regions owing to the accumulation of various defects. Incident-ion-induced strains originate from ion implantation regions at the end of the ion range. As the ion fluence successively increased to a relatively higher value, defect evolution and stress release occurred, leading to a slow increase in strain. The first term in Eq. (2) can be attributed to defect-related strains caused by displacement damage owing to nuclear energy deposition. The second term in Eq. (2) can be ascribed to lattice deformation-induced strains owing to the addition of incident ions. The coefficient of ϕ is considered as the damage cross section in Eq. (2). Comparing the fitted data in Eq. (2), we found that the damage cross section of the first term (−39.53) is much larger than that of the second term (−3.573) in Eq. (2). Therefore, we can conclude that the defect characteristics caused by nuclear energy loss play a significant role in the changes in strain.

To confirm the strain changes induced by defect evolution further, we estimated the dislocation density (δ) parameter from the HRXRD curves using an equation that describes the relationship between the shape and broadening of the diffraction peaks and the density of dislocations within a crystal lattice [43]. This analysis provides insight into the strain changes induced by defect evolution within the crystal structure. The equation form is as follows [43]:

$$\delta = 1/D^2, \quad (3)$$

where D is the thickness of the diffraction layer in the GaN(0002) plane. Fitting the HRXRD curves (Fig. 2), the full width at half maximum (FWHM) and Bragg angle of the diffraction peak of the GaN(0002) lattice plane were determined. The value of D was obtained using an empirical Scherrer equation. D was calculated from the HRXRD curves in a previous study [44]. For the un-irradiated GaN specimen, its value is approximately (178.6558 ± 7.146) nm. After Kr^{19+} ion irradiation at fluences of 1.0×10^{11}, 1.0×10^{12}, and 1.0×10^{13} Kr ions/cm^2, the corresponding thicknesses of the diffraction layer (D) were approximately (135.3325 ± 6.7666), (115.1562 ± 4.6062), and (59.3774 ± 2.9688) nm, respectively. Meanwhile, for Ne^{8+} ion irradiation at fluences of 1.0×10^{11}, 1.0×10^{12}, 1.0×10^{13}, 1.0×10^{14}, and 1.0×10^{15} Ne ions/cm^2, the corresponding thicknesses of the diffraction layer (D) were approximately (171.2225 ± 6.489), (168.0248 ± 8.4012), (112.5115 ± 4.5004), (23.9323 ± 1.1966), and (22.8045 ± 1.1402) nm, respectively. The dislocation density parameter (δ) was also calculated at different fluences for the two types of ion irradiation. For the un-irradiated GaN specimen, the value of the dislocation density parameter (δ) was approximately $(3.1330 \pm 0.1253) \times 10^{-5}$ lines/nm^2. After Kr^{19+} ion irradiation, dislocation density parameters (δ) with values of approximately $(5.4600 \pm 0.2184) \times 10^{-5}$, $(7.5409 \pm 0.3770) \times 10^{-5}$, and $(28.363 \pm 1.134) \times 10^{-5}$ lines/nm^2 were calculated, corresponding to 1.0×10^{11}, 1.0×10^{12}, and 1.0×10^{13} Kr ions/cm^2 irradiation, respectively. Clearly, as the irradiation fluence successively increased to 1.0×10^{12} Kr^{19+}/cm^2, the average dislocation density slowly increased from $(3.1330 \pm 0.1253) \times 10^{-5}$ to $(7.5409 \pm 0.3770) \times 10^{-5}$ lines/nm^2. Above this fluence, the average dislocation density rapidly increased to $(28.363 \pm 1.134) \times 10^{-5}$ lines/nm^2. After Ne^{8+} ion irradiation at fluences of 1.0×10^{11}, 1.0×10^{12}, 1.0×10^{13}, 1.0×10^{14}, and 1.0×10^{15} Ne ions/cm^2, the corresponding values of the average dislocation density were approximately $(3.4109 \pm 0.1705) \times 10^{-5}$, $(3.5420 \pm 0.1416) \times 10^{-5}$, $(7.8996 \pm 0.3949) \times 10^{-5}$, $(175.2 \pm 7.031) \times 10^{-5}$, and $(192.3 \pm 9.011) \times 10^{-5}$ lines/nm^2. When the irradiation fluence was successively increased to 1.0×10^{13} Ne^{8+}/cm^2, the average dislocation density slowly increased from $(3.1330 \pm 0.1253) \times 10^{-5}$ to $(7.8996 \pm 0.3949) \times 10^{-5}$ lines/nm^2. When the ion fluence increased to 1.0×10^{14} Ne^{8+}/cm^2, the

average dislocation density sharply increased to $(1.752 \pm 0.07031) \times 10^{-3}$ lines/nm^2. As the irradiation fluence was further increased to 1.0×10^{15} Ne^{8+}/cm^2, the average dislocation density gradually increased to $(1.923 \pm 0.09011) \times 10^{-3}$ lines/nm^2. Generally, as the ion fluence increased successively, similar changes in the dislocation density were observed for the two types of ion-irradiated GaN films. These results indicated that the disordered regions and distorted lattice planes increased with increasing ion fluences in the irradiated GaN films owing to defect accumulation. Consequently, the amorphous rate of the GaN films was enhanced. It should be noted that a conflicting trend appeared between the lattice strains and the dislocation density with ion fluences (Fig. 3). Based on the data presented in Fig. 3 and the above-mentioned dislocation density, we can conclude that the dislocation density increases sharply during the process of strain release.

Additionally, to provide further insight into the structural changes induced by MeV energy ion irradiation and to understand the overall strain behavior of the GaN films under different conditions, the distortion parameters (g) of all the specimens, including the un-irradiated and irradiated GaN films, were calculated from the HRXRD curves based on the following specific formula [45]:

$$g = \beta/\tan(\theta), \tag{4}$$

where β is the FWHM of GaN(0002) diffraction peak and θ describes the Bragg diffraction angle of the GaN(0002) main peak. For the un-irradiated GaN specimen, the calculated value of the distortion parameter was approximately $(3.216 \pm 0.128)\%$. After Kr^{19+} ion irradiation with fluences of 1.0×10^{11}, 1.0×10^{12}, and 1.0×10^{13} Kr ions/cm^2, the corresponding values of the distortion parameter were approximately $(4.046 \pm 0.202)\%$, $(4.648 \pm 0.185)\%$, and $(9.007 \pm 0.450)\%$, respectively. Meanwhile, for Ne^{8+} irradiation, distortion parameters with approximate values of $(3.319 \pm 0.165)\%$, $(3.373 \pm 0.168)\%$, $(3.493 \pm 0.139)\%$, $(13.11 \pm 0.655)\%$, and $(13.15 \pm 0.526)\%$ were estimated, corresponding to 1.0×10^{11}, 1.0×10^{12}, 1.0×10^{13}, 1.0×10^{14}, and 1.0×10^{15} irradiation, respectively. It is evident that the distortion parameters increase with increasing ion fluences. This confirms the formation of disordered structures in the irradiated GaN films. Furthermore, the dislocation density (δ) and distortion parameters (g) exhibit the same trend with respect to the ion fluences for both ion irradiations. As the irradiation fluence successively increased to 1.0×10^{12} Kr^{19+}/cm^2, the average distortion parameters slowly increased from $(3.216 \pm 0.128)\%$ to $(4.648 \pm 0.185)\%$. Above this fluence, the average distortion parameter rapidly increased to $(9.007 \pm 0.450)\%$. For Ne^{8+} ion irradiation, when the irradiation fluence successively increased to 1.0×10^{13} Ne^{8+}/cm^2, the average distortion parameters slowly increased from $(3.216 \pm 0.128)\%$ to $(3.493 \pm 0.139)\%$. When the ion fluence increased to 1.0×10^{14} Ne^{8+}/cm^2, the average distortion parameters sharply increased to $(13.11 \pm 0.655)\%$. As the irradiation fluence further rose up to 1.0×10^{15} Ne^{8+}/cm^2, the average distortion parameters gently increased to $(13.15 \pm 0.526)\%$. It is worth mentioning that during the distortion process, the parameters increased remarkably, and as stated above, the lattice strains underwent a transition from a rapid increase to a mild increase (Fig. 3). This can be attributed to the release of lattice stress via the migration and rearrangement of dislocations and stacking faults, as a result of which the strain energy is consumed by material deformation, cracks, and fractures.

3.2 UV–Vis Spectrum

Bandgap energy is a vital optical parameter for semiconductor materials (GaN). To investigate the effects of lattice strains caused by irradiation on the bandgap energy, we carried out UV–Vis transmittance spectrum analysis on the irradiated GaN films. Figure 4a and b shows the UV–Vis transmittance spectrum curves of GaN films irradiated with 5.3-MeV $Kr^{19+}$and 2.3-MeV Ne^{8+} ions, respectively, at different fluences. Figure 4 shows that with an increase in ion fluence, the transmissivity of GaN films decreases for the two types of ion irradiation. This is due to the enhancement in the absorption and scattering of defects induced by irradiation. Simultaneously, a wide interference band appears owing to the interface between the GaN film and its substrate (Al_2O_3). Moreover, the shape of the optical absorption edge in the GaN films gradually becomes oblique with respect to the ion fluence. This change is ascribed to the introduction of absorption structures within the bandgap. In particular, this alteration in the band edge absorption of irradiated GaN films is attributed to the introduction of additional electronic energy states [46]. These states are likely a consequence of the structural changes induced by irradiation, such as the creation of various defects in the material. Overall, these observations highlight the complex interplay between lattice stresses, irradiations, and the optical and electronic properties of GaN films. The mechanisms involved have significant implications for the performance and reliability of GaN-based devices and materials. Tauc's formula [47] was used to estimate the optical bandgap energy (E_g) as follows:

$$\alpha h\nu = A(h\nu - E_g)^n, \tag{5}$$

where α is the absorption coefficient, which can be calculated from the UV–Vis transmittance curve. $h\nu$ is the photon's energy computed as $h\nu = 1240/\lambda$. A is a constant correlated with the refractivity, reduced mass, and absorption brink width. Additionally, n represents the optical transition

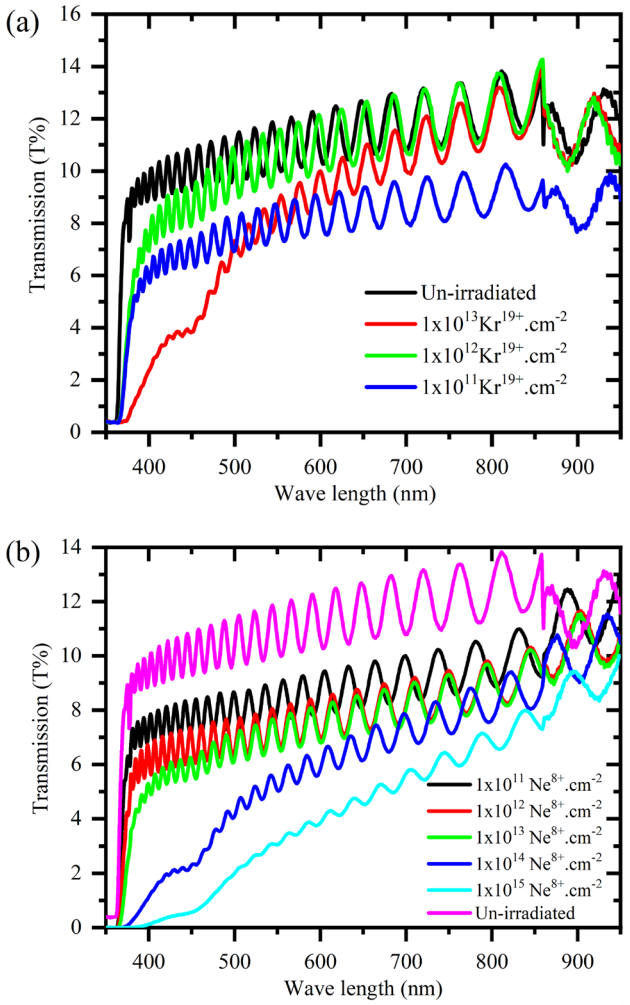

Fig. 4 (Color online) UV–Vis transmittance spectrum curves of GaN films irradiated with (**a**) 5.3-MeV Kr^{19+} ions and (**b**) 2.3-MeV Ne^{8+} ions at different fluences

phase. For direct bandgap semiconductor materials (GaN), the value of n was set to 1/2.

Using this formula [47], the optical bandgap energy (E_g) of GaN films can be deduced from the $(\alpha h\nu)^2$ versus ($h\nu$) plots. The bandgap energies of all GaN films, including the un-irradiated, Kr^{19+} ion-irradiated, and Ne^{8+} ion-irradiated specimens, were computed based on the above formula [47]. The bandgap energy of the un-irradiated GaN specimen is approximately (3.3562 ± 0.1667) eV. After Kr^{19+} ion irradiation at a fluence of 1.0×10^{11}, 1.0×10^{12}, and 1.0×10^{13} Kr ions/cm^2, the corresponding values of the bandgap energy (E_g) were approximately (3.2645 ± 0.1632), (3.2372 ± 0.1618), and (2.9394 ± 0.1469) eV under approximate lattice strains of 0.005%, 0.06%, and 0.32%, respectively. Meanwhile, for Ne^{8+} ion irradiation with fluences of 1.0×101^{11}, 1.0×10^{12}, 1.0×10^{13}, 1.0×10^{14}, and 1.0×10^{15} Ne ions/cm^2, the corresponding bandgap energy (E_g) values of GaN films were approximately (3.3513 ± 0.1675), (3.3245 ± 0.1662), (3.2916 ± 0.1645), (2.9258 ± 0.1629), and (2.8645 ± 0.1617) eV under approximate lattice strains of 0, 0.008%, 0.06%, 0.44%, and 0.68%, respectively. When the ion fluence was enhanced, the bandgap energy of the GaN films decreased, accompanied by an increase in the lattice strain. After Kr^{19+} ion irradiation, its value gradually decreased from (3.3562 ± 0.1667) to (2.9394 ± 0.1469) eV. As the ion fluence increased up to 1.0×10^{12} Kr ions/cm^2, the optical bandgap energy of GaN films decreased to (3.2372 ± 0.1618) eV, with a rapid increase in strains from 0.005% to 0.06%. Above this fluence, its value sharply decreased to (2.9394 ± 0.1469) eV under a strain value of approximately 0.32%. Similar changes in bandgap energy were observed in Ne^{8+} ion-irradiated GaN specimens. The value of optical bandgap energy decreased from (3.3562 ± 0.1667) to (2.8645 ± 0.1617) eV after Ne^{8+} ion irradiation. When the ion fluence was lower than 1.0×10^{13} Ne^{8+}/cm^2, the bandgap energy slowly reduced to (3.2916 ± 0.1645) eV after the lattice strain rapidly increased to 0.06%. Above this fluence, the bandgap energy rapidly decreased to (2.9258 ± 0.1629) eV and the strain enhanced to 0.44% from 0.06%. As the irradiation fluence further increased up to 1.0×10^{15} Ne ions/cm^2, its value decreased to (2.8645 ± 0.1617) eV under a slow increase in lattice strain from 0.44% to 0.68%. The interaction of ions with GaN films caused various defects in the bandgap, resulting in a reduction in the optical bandgap energy. In other words, the generation of defects led to the establishment of localized states between the valence and conduction bands, which reduced the bandgap energy [48]. In addition, for lower fluence irradiation, a slow reduction in bandgap energy was observed owing to the generation of single defects and accumulation of strain. At a relatively higher fluence irradiation for both ions, the observed significant reduction in the bandgap energy of the irradiated GaN films was attributed to the creation of dislocations, lattice distortions, and stacking faults due to strain release. In general, these results agree well with the HRXRD analysis.

However, the exponential shape of the optical absorption edge in the UV–Vis spectrum reflects the structural disorder in dielectrics and semiconductors [49–51]. Some research groups have investigated disordered and amorphous materials using the Urbach energy obtained from the absorption edge of the UV–Vis spectrum curves [52–55]. The Urbach energy has been successfully applied to characterize the total structural disorder in ion- and neutron-irradiated crystals and glasses, as well as in thin films and nanoparticles [53–55]. This enabled us to clarify the atomic disorder levels using qualitative and quantitative methods based on the shapes of the formed spectral curves. Similarly, lattice disorders in

crystalline semiconductors (GaN) induced by ion irradiation can be characterized by the Urbach energy. The irradiation-dependent Urbach energy was deduced from the absorption spectra.

The absorption coefficient (α) can be achieved from the UV–Vis spectrum and α is characterized using the following equation [48]:

$$\alpha(\nu) = \alpha_{o} e^{h\nu/E_{u}}, \tag{6}$$

where E_u is the Urbach energy (Urbach bandtail). This can be calculated by plotting the absorption coefficient ($\ln \alpha$) versus photon energy ($h\nu$). E_u characterizes the static and dynamic disorders in materials and embodies the state density tail length at the energy band boundary. Its boundary is located at the onset of a sharp drop in transmittance in the UV–Vis curves shown in Fig. 4.

Based on the UV–Vis curves shown in Fig. 4, we found that the energy band boundary of the un-irradiated GaN specimen was approximately 3.28 eV. For Kr^{19+} ion-irradiated GaN specimens, the values of the energy band boundary were approximately 3.12, 2.97, and 2.78 eV, corresponding to 1.0×10^{11}, 1.0×10^{12}, and 1.0×10^{13} Kr^{19+}/cm^2, respectively (Fig. 4a). Meanwhile, for Ne^{8+} ion-irradiated GaN specimens with fluences of 1.0×10^{11}, 1.0×10^{12}, 1.0×10^{13}, 1.0×10^{14}, and 1.0×10^{15} Ne ions/cm^2, the corresponding values of the energy band boundary were approximately 3.28, 3.26, 3.23, 2.59, and 2.42 eV, respectively (Fig. 4b). Near the energy band boundary, E_u can be computed using $\ln \alpha \sim h\nu$ plots. The E_u values of all GaN films, including those un-irradiated and those irradiated with two types of ions at different fluences, were computed. The Urbach energy of the non-irradiated GaN film was approximately (0.1735 ± 0.0086) eV. After Kr^{19+} ion irradiation at fluences of 1.0×10^{11}, 1.0×10^{12}, and 1.0×10^{13} Krions/cm^2, the corresponding values of Urbach energy were (0.3056 ± 0.0152), (0.3075 ± 0.0153), and (0.3307 ± 0.0165) eV under approximate lattice strains of 0.005%, 0.06%, and 0.32%, respectively. Meanwhile, for Ne^{8+} ion irradiation, the values of Urbach energy were (0.2887 ± 0.0144), (0.2953 ± 0.0147), (0.3122 ± 0.0156), (0.3401 ± 0.0170), and (0.3526 ± 0.0176) eV, corresponding to fluences of 1.0×10^{11}, 1.0×10^{12}, 1.0×10^{13}, 1.0×10^{14}, and 1.0×10^{15} Ne^{8+}/cm^2 irradiation, with approximate lattice strains of 0, 0.008%, 0.06%, 0.44%, and 0.68%, respectively. Obviously, the Urbach energy increased with respect to lattice strains and ion fluences after the GaN films were irradiated by the two types of ions with different fluences. This occurs because disorder is created and localized states are formed owing to irradiation [56, 57]. However, we found that as the Kr^{19+} ion fluence increased to 1.0×10^{12} Kr ions/cm^2, the Urbach energy slowly increased from (0.1735 ± 0.0086) to (0.3075 ± 0.0153) eV, with a rapid increase in strains from 0.005 to 0.06%. When the irradiation fluence further increased to 1.0×10^{13} Kr ions/cm^2, the values of Urbach energy significantly increased to (0.3307 ± 0.0165) eV under a slow increase to 0.32% from 0.06% in lattice strain value. Ne^{8+} ion-irradiated GaN specimens showed similar change to that obtained with Kr^{19+} ions. As the fluence was lower than 1.0×10^{13} Ne^{8+}/cm^2, the Urbach energy also slowly increased from (0.1735 ± 0.0086) to (0.3122 ± 0.0156) eV after the lattice strain rapidly increased up to 0.06%. Above this fluence, its value sharply increases to (0.3401 ± 0.0170) eV. In this case, the strain value increased slowly to 0.44%. As its fluence further increased to 1.0×10^{15} Ne^{8+}/cm^2, the Urbach energy value mildly increased to (0.3526 ± 0.0176) eV under a strain value of 0.68%. These results were consistent with those reported by other research groups [58, 59]. It should be noted that when the irradiation fluence exceeded a certain value, the significant increase in Urbach energy was ascribed to the production of dislocations, lattice distortions, and stacking faults owing to the release of strains. This result is in good agreement with the average distortion parameters and dislocation densities deduced from the HRXRD curves. According to Fig. 3 and the computed data (average distortion, dislocation density, bandgap energy, and Urbach energy), we can conclude that severe lattice damage occurs and the defect concentration remarkably increases during the process of strain release. This leads to a significant decrease in the optical bandgap energy and an evident increase in Urbach energy.

4 Conclusion

The strain-related defect evolution and band edge characteristics of GaN films irradiated with 2.3-MeV Ne^{8+} and 5.3-MeV Kr^{19+} ions at different fluences were investigated using HRXRD and UV–Vis spectroscopy. The results revealed that damage accumulations and lattice strains are mainly caused by nuclear energy loss, whereas energy loss via electronic processes contribute less to GaN crystal damage. Moreover, the lattice strain is composed of two main parts: defect-induced and incident-ion-induced strains. The strain caused by defects is the principal component. Because the ion fluence is less than ~ 0.055 dpa, the defects in GaN are mainly simple point defects, whose concentration is approximately linearly proportional to the total nuclear energy loss. This results in a rapid enhancement of lattice strains with ion fluences. Simultaneously, in this case, the dislocation density, distortion parameter, and Urbach energy generally displayed a slow increase with increasing ion fluences for both ion irradiations. When the irradiation fluence exceeded ~ 0.055 dpa, a slow increase in the lattice strains was observed, accompanied by a rapid increase in the dislocation density, distortion

parameter, and Urbach energy with respect to the ion fluences. This occurs because the concentration of point defects becomes saturated and more complicated defects (dislocations and stacking faults) begin to form in the irradiated GaN films owing to strain release. It is suggested that ~ 0.055 dpa is a threshold value of defect evolution from point defects to complicated defects; meanwhile, it also is a threshold value of stress release in GaN materials. Our results may serve as a reference for GaN-based devices to be utilized fully in radiative environments.

Author contributions All authors contributed to the study conception and design. Material preparation, data collection, and analysis were performed by Yang Gao, Shuang Liu, Qin-Wei Wang, Ya-Xun Zhang, Rui Li, Lei Zhou, Qiang Zhou, Chen-Chun Hao, and Rong Qiu. The first draft of the manuscript was written by Li-Qing Zhang and Chong-Hong Zhang, and all authors commented on previous versions of the manuscript. All authors read and approved the final manuscript.

Data availability The data that support the findings of this study are openly available in Science Data Bank at https://cstr.cn/31253.11.sciencedb.j00186.00847 and https://www.doi.org/10.57760/sciencedb.j00186.00847.

Declarations

Conflict of interest The authors declare that they have no conflict of interest.

References

1. Z.X. Qin, Z.Z. Chen, H.X. Zhang et al., Effect of O_2/CHF_3 plasma treatment on n-type GaN grown on sapphire by MOCVD. Mat. Sci. Semicon. Proc. **5**, 473–475 (2003). https://doi.org/10.1016/S1369-8001(03)00048-9
2. X.Y. Li, J.B. Lu, Y.M. Liu et al., Exploratory study of betavoltaic battery using ZnO as the energy converting material. Nucl. Sci. Tech. **30**, 60 (2019). https://doi.org/10.1007/s41365-019-0577-3
3. A.H. Liu, Impulse-coupling coefficients from a pulsed-laser ablation of semiconductor GaAs. Nucl. Sci. Tech. **17**, 217–221 (2006). https://doi.org/10.1016/S1001-8042(06)60040-7
4. L.C. Wei, S.L. Bao, Q.X. Yang et al., Lattice locations determination of trace amount carbon in gallium arsenide by theoretical calculation of CPAA with channeling. Nucl. Sci. Tech. **2**, 211–219 (1991) http://www.nst.sinap.ac.cn/article/id/5979
5. C.C. Chen, Z.H. Liu, W.T. Huang et al., The property of Si/SiGe/Si heterostructure during thermal budget characterized by HRXRD. Nucl. Sci. Tech. **14**, 238–241 (2003) http://qikan.cqvip.com/Qikan/Article/Detail?id=9232514
6. D. Zhu, D.J. Wallis, C.J. Humphreys, Prospects of III-nitride optoelectronics grown on Si. Rep. Prog. Phys. **76**, 106501 (2013). https://doi.org/10.1088/0034-4885/76/10/106501
7. Y.H. Lin, S.Z. Zhou, W.L. Wang et al., Performance improvement of GaN-based light emitting diodes grown on Si(111) substrates by controlling the reactor pressure for the GaN nucleation layer growth. J. Mater. Chem. C. **3**, 1484–1490 (2015). https://doi.org/10.1039/C4TC02220C
8. G.Q. Li, W.L. Wang, W.J. Yang et al., Epitaxial growth of group III-nitride films by pulsed laser deposition and their use in the development of LED devices. Surf. Sci. Rep. **70**, 380–423 (2015). https://doi.org/10.1016/j.surfrep.2015.06.001
9. W.L. Wang, H.Y. Wang, W.J. Yang et al., A new approach to epitaxially grow high-quality GaN films on Si substrates: the combination of MBE and PLD. Sci. Rep. **6**, 24448 (2016). https://doi.org/10.1038/srep24448
10. D. Verheij, M. Peres, S. Cardoso et al., Radiation sensors based on GaN microwires. J. Phys. D Appl. Phys. **51**, 175105 (2018). https://doi.org/10.1088/1361-6463/aab636
11. M.L. Zhang, R.X. Yang, Z.X. Li et al., Study on proton irradiation induced defects in GaN thick film. Acta. Phys. Sin. **62**, 425–428 (2013). https://doi.org/10.7498/aps.62.117103
12. P. Kavouras, P. Konminou, T. Karakostas, Effects of ion implantation on the mechanical behavior of GaN films. Thin Solid Films **515**, 3011–3018 (2007). https://doi.org/10.1016/j.tsf.2006.08.032
13. Y. Zhang, M. Ishimaru, J. Jagielski et al., Damage and microstructure evolution in GaN under Au ion irradiation. J. Phys. D Appl. Phys. **43**, 085303 (2010). https://doi.org/10.1088/0022-3727/43/8/085303
14. H.X. Li, Y.X. Lu, T. Zhu et al., Impact of gamma-ray irradiation on photo emission from InGaN/GaN LED. Microelectron. Reliab. **142**, 114915 (2023). https://doi.org/10.1016/j.microrel.2023.114915
15. S.J. Pan, S.W. Feng, X. Li et al., Analysis of the effects of high-energy electron irradiation of GaN high-electron-mobility transistors using the voltage-transient Method. Ieee. T. Electron. Dev. **68**, 3968–3973 (2021). https://doi.org/10.1109/TED.2021.3089449
16. L.Q. Zhang, C.H. Zhang, C.L. Xu et al., Damage produced on GaN surface by highly charged Kr^{q+} irradiation. Nucl. Sci. Tech. **28**, 176 (2017). https://doi.org/10.1007/s41365-017-0326-4
17. S.L. Chen, Atomic displacement damage energy model up to high recoil energy. Nucl. Instrum. Methods Phys. Res. B. **536**, 104–112 (2023). https://doi.org/10.1016/j.nimb.2023.01.007
18. C.H. Zhang, Y. Song, Y.M. Sun et al., Damage accumulation in gallium nitride irradiated with various energetic heavy ions. Nucl. Instrum. Methods Phys. Res. B. **256**, 199–206 (2007). https://doi.org/10.1016/j.nimb.2006.12.003
19. M.F. Wu, S.Q. Zhou, S.D. Yao et al., High precision determination of the elastic strain of InGaN/GaN multiple quantum wells. J. Vac. Sci. Technol. B **22**, 920–924 (2004). https://doi.org/10.1116/1.1715085
20. A. Pandey, R. Raman, S. Dalal et al., Structural and optical characteristics investigations in oxygen ion implanted GaN epitaxial layers. Mat. Sci. Semicon. Proc. **107**, 104833 (2020). https://doi.org/10.1016/j.mssp.2019.104833
21. L.M. Zhang, C.H. Zhang, L.Q. Zhang et al., Structural and optical study of irradiation effect in GaN epilayers induced by 308 MeV Xe ions. Nucl. Instrum. Methods Phys. Res. B. **269**, 1782–1785 (2011). https://doi.org/10.1016/j.nimb.2011.04.118
22. Q.Z. Ji, M. Yang, Q.D. Cheng et al., Study on proton irradiation effect of GaN optical and electrical properties. J. Korean Soc. **83**, 372–380 (2023). https://doi.org/10.1007/s40042-023-00864-0
23. J. Huang, K. Xu, Y.M. Fan et al., Dislocation luminescence in GaN single crystals under nanoindentation. Nanoscale Res. Lett. **9**, 649 (2014). https://doi.org/10.1186/1556-276X-9-649
24. L.Q. Zhang, C.H. Zhang, J.J. Li et al., Damage to epitaxial GaN layer on Al_2O_3 by 290-MeV $^{238}U^{32+}$ ions irradiation. Sci. Rep. **8**, 4121 (2018). https://doi.org/10.1038/s41598-018-22321-w
25. L. Lv, X.H. Ma, J.C. Zhang et al., Proton irradiation effects on AlGaN/AlN/GaN heterojunctions. IEEE Trans. Nucl. Sci. **62**, 300–305 (2015). https://doi.org/10.1109/TNS.2014.2374178
26. L. Wang, N.Y. Liu, B. Li et al., Comparison of X-ray and proton irradiation effects on the characteristics of InGaN/GaN multiple quantum wells light-emitting diodes. IEEE Trans. Nucl. Sci. **67**, 1345–1350 (2020). https://doi.org/10.1109/TNS.2020.2975002
27. L.Q. Zhang, C.H. Zhang, C.L. Xu et al., Influence of highly-charged $^{209}Bi^{33+}$ irradiation on structure and optoelectric

characteristics of GaN epilayer. Nucl. Instrum. Methods Phys. Res. B. **406**, 571–577 (2017). https://doi.org/10.1016/j.nimb.2017.04.056
28. P.P. Hu, J. Liu, S.X. Zhang et al., Raman investigation of lattice defects and stress induced in InP and GaN films by swift heavy ion irradiation. Nucl. Instrum. Methods Phys. Res. B. **372**, 29–37 (2019). https://doi.org/10.1016/j.nimb.2016.01.031
29. L.J. Huang, L. Li, Z. Shang et al., Structure and luminescence of a-plane GaN on r-plane sapphire substrate modified by Si implantation. Chin. Phys. B **30**, 63–68 (2021). https://doi.org/10.1088/1674-1056/abd76a
30. G.P. Liu, X. Wang, M.N. Li et al., Effects of high-energy proton irradiation on separate absorption and multiplication GaN avalanche photodiode. Nucl. Sci. Tech. **29**, 155–162 (2018). https://doi.org/10.1007/s41365-018-0480-3
31. Z. Bi, J.C. Zhang, L. Lv et al., The effect of 3-MeV proton irradiation on the performance of inGaN/GaN MQWs solar cells. IEEE Photon. Technol. Lett. **26**, 1492–1494 (2014). https://doi.org/10.1109/LPT.2014.2327072
32. Z.H. Dong, X.Y. Zhang, J.L. Li et al., Effects of ion irradiation and temperature on mechanical properties of GaN single crystals under nanoindentation. Materials **16**, 7537 (2023). https://doi.org/10.3390/ma16247537
33. L.Q. Zhang, C.H. Zhang, Y.Q. Xian et al., Degradation mechanisms of optoelectric properties of GaN via highly-charged $^{209}Bi^{33+}$ ions irradiation. Appl. Sur. Sci. **440**, 814–820 (2018). https://doi.org/10.1016/j.apsusc.2018.01.170
34. J.F. Ziegler, J.P. Biersack, U. Littmark, *The Stopping and Range of Ions in Matter* (Pergamon, New York, 1985)
35. D.C. Look, D.C. Reynolds, J.W. Hemsky, Defect donor and acceptor in GaN. Phys. Rev. Lett. **79**, 2273–2273 (1997). https://doi.org/10.1063/1.120059
36. C. Liu, B. Mensching, K. Volz et al., Lattice expansion of Ca and Ar ion implanted GaN. Appl. Phys. Lett. **71**, 2313–2315 (1997). https://doi.org/10.1063/1.120059
37. M.F. Wu, S.Q. Zhou, S.D. Yao et al., High precision determination of the elastic strain of InGaN/GaN multiple quantum wells. J. Vac. Sci. Technol. B **22**, 920–924 (2004). https://doi.org/10.1116/1.1715085
38. E. Oliviero, M.L. David, M. Beaufort et al., Formation of bubbles by high dose He implantation in 4H-SiC. J. Appl. Phys. **91**, 1179–1186 (2002). https://doi.org/10.1063/1.1429760
39. M.W. Dashiell, G. Xuan, E. Ansorge et al., Pseudomorphic SiC alloys formed by Ge ion implantation. Appl. Phys. Lett. **85**, 2253–2255 (2004). https://doi.org/10.1063/1.1791741
40. S. Pereira, M.R. Correia, E. Pereira, Strain and composition distributions in wurtzite InGaN/GaN layers extracted from X-ray reciprocal space mapping. Appl. Phys. Lett. **80**, 3913–3915 (2002). https://doi.org/10.1063/1.1481786
41. M.A. Moram, M.E. Vickers, X-ray diffraction of III-nitrides. Rep. Prog. Phys. **72**, 036502 (2009). https://doi.org/10.1088/0034-4885/72/3/036502
42. S.B. Qadri, B. Molnar, M. Yousuf et al., X-ray determination of strain in ion implanted GaN. Nucl. Instrum. Methods Phys. Res. B. **190**, 878–881 (2002). https://doi.org/10.1016/S0168-583X(01)01189-2
43. A. Abdel-Galil, A. Atta, M. Balboul, Effect of low-energy oxygen ion beam treatment on the structural and physical properties of ZnO thin films. Surf. Rev. Lett. **27**, 2050019 (2020). https://doi.org/10.1142/S0218625X20500195
44. L.Q. Zhang, C.H. Zhang, X.J. Jia et al., Structures and optical properties of Kr^{23+} and Ne^{8+}-irradiated GaN epi-layers. Nucl. Instrum Methods Phys. Res. B. **307**, 60–64 (2013). https://doi.org/10.1016/j.nimb.2012.12.101
45. A. Atta, M.M. Abdelhamied, A.M. Abdelreheem et al., Flexible methyl cellulose/polyaniline/silver composite films with enhanced linear and nonlinear optical properties. Polymers **13**, 1225 (2021). https://doi.org/10.3390/polym13081225
46. C. Rao, M. Ravi, V. Raja et al., Preparation and characterization of PVP-based polymer electrolytes for solid-state battery applications. Iran. Polym. J. **21**, 531–536 (2012). https://doi.org/10.1007/s13726-012-0058-6
47. A. Atta, A.M. Abdel reheem, E. Abdeltwab, Ion beam irradiation effects on surface morphology and optical properties of ZnO/PVA composites. Surf. Rev. Lett. **27**, 1950214 (2020). https://doi.org/10.1142/S0218625X19502147
48. M.F. Zaki, A.M. Ali, R.M. Amin, Effect of gamma irradiation on optical and chemical properties of cellulose nitrate thin films. J. Adhes. Sci. Technol. **31**, 1314–1327 (2017). https://doi.org/10.1080/01694243.2016.1255455
49. J. Tauc, H. Grigorovici, A. Vancu, Optical properties and electronic structure of amorphous germanium. Phys. Status Solidi **15**, 627 (1966). https://doi.org/10.1002/pssb.19660150224
50. G.D. Cody, T. Tiedje, B. Abeles et al., Disorder and the optical-absorption edge of hydrogenated amorphous silicon. Phys. Rev. Lett. **47**, 1480 (1981). https://doi.org/10.1103/PhysRevLett.47.1480
51. N.F. Mott, E.A. Davis, *Electronic Processes in Non-Crystalline Materials* (Oxford University Press, Oxford, 1979)
52. I.A. Vainshtein, A.F. Zatsepin, V.S. Kortov et al., The urbach rule for the PbO-SiO_2 glasses. Phys. Solid State **42**, 230–235 (2000). https://doi.org/10.1134/1.1131151
53. A.F. Zatsepin, Y.A. Kuznetsova, V.I. Sokolov, UV absorption and effects of local atomic disordering in the nickel oxide nanoparticles. J. Lumin. **183**, 135–142 (2017). https://doi.org/10.1016/j.jlumin.2016.11.006
54. A. Zatsepin, Y. Kuznetsova, D. Zatsepin et al., Electronic structure and optical absorption in Gd-implanted silica glasses. Phys. Status Solidi A **216**, 1800522 (2018). https://doi.org/10.1002/pssa.201800522
55. I.A. Vainshtein, A.F. Zatsepin, V.S. Kortov, Quasi-dynamic structural disorder induced by fast neutrons in $Be_3Al_2Si_6O_{18}$ crystals. Phys. Solid State **43**, 246–250 (2001). https://doi.org/10.1134/1.1349468
56. H.M. Zeyada, M.M. EL-Nahass, M.M. EL-Shabaan, Gamma-ray irradiation induced structural and optical constants changes of thermally evaporated neutral red thin films. J. Mater. Sci. **47**, 493–502 (2012). https://doi.org/10.1007/s10853-011-5825-9
57. M.M. Abdelhamied, A. Atta, A.M. Abdelreheem et al., Oxygen ion induced variations in the structural and Linear/Nonlinear optical properties of the PVA/PANI/Ag nanocomposite film. Inorg. Chem. Commun. **133**, 108926 (2021). https://doi.org/10.1016/j.inoche.2021.108926
58. C. Kaiser, O.J. Sandberg, N. Zarrabi et al., A universal Urbach rule for disordered organic semiconductors. Nat. Commun. **12**, 3988 (2021). https://doi.org/10.1038/s41467-021-24202-9
59. A.F. Zatsepin, D.Y. Biryukov, N.V. Gavrilov et al., Induced quasi-dynamic disorder in a structure of rhenium ion-implanted quartz glass. Phys. Solid State **61**, 1017–1022 (2019). https://doi.org/10.1134/S1063783419060301